



OPEN ACCESS

EDITED BY

Yugao Ma,
Nuclear Power Institute of China (NPIC), China

REVIEWED BY

Yonghee Kim,
Korea Advanced Institute of Science and
Technology (KAIST), Republic of Korea
Shanfang Huang,
Tsinghua University, China
Xiang Wang,
Harbin Engineering University, China

*CORRESPONDENCE

Hui Guo,
✉ maxime.guohui@foxmail.com

RECEIVED 29 November 2023

ACCEPTED 25 January 2024

PUBLISHED 06 February 2024

CITATION

Feng K, Hu J, Wang Y, Cong T, Gu H and Guo H
(2024), Multiphysics analysis of a metal hydride
moderated megawatt heat pipe reactor with
burnable poisons.
Front. Energy Res. 12:1346311.
doi: 10.3389/fenrg.2024.1346311

COPYRIGHT

© 2024 Feng, Hu, Wang, Cong, Gu and Guo.
This is an open-access article distributed under
the terms of the [Creative Commons Attribution
License \(CC BY\)](https://creativecommons.org/licenses/by/4.0/). The use, distribution or
reproduction in other forums is permitted,
provided the original author(s) and the
copyright owner(s) are credited and that the
original publication in this journal is cited, in
accordance with accepted academic practice.
No use, distribution or reproduction is
permitted which does not comply with these
terms.

Multiphysics analysis of a metal hydride moderated megawatt heat pipe reactor with burnable poisons

KuaiYuan Feng, Jipu Hu, Yihu Wang, Tenglong Cong, Hanyang Gu and Hui Guo*

School of Nuclear Science and Engineering, Shanghai Jiao Tong University, Shanghai, China

With the development of nuclear energy, microreactors have received increasing interest among researchers in recent years. In this paper, a megawatt heat pipe reactor with metal hydride moderators and burnable poisons is proposed. The hydrogen stability of the reactor under accident conditions, including reactivity insertion accidents, loss of power conversion unit heat sink accidents, and heat pipe failure accidents are analyzed. In this work, Gd_2O_3 is introduced as a burnable poison in the form of mixing with the UO_2 fuel. According to the results of the burnable poison design, the 0.1% mass fraction of Gd_2O_3 is selected as the burnable poison loaded in the core. Safety analysis indicates that the introduction of burnable poisons can be beneficial during the positive reactivity insertion accident as it can reduce the excessive reactivity at BOL, thus reducing power peak and preventing hydrogen dissociation in $ZrH_{1.4}$ rods. However, during the loss of PCU heat sink accident, $ZrH_{1.4}$ rods will dissociate regardless of the presence of burnable poisons, whereas $YH_{1.7}$ rods show better hydrogen stability. Moreover, in the event of the heat pipe failure accident, $ZrH_{1.4}$ rods are more susceptible to dissociation than $YH_{1.7}$ rods. As a result, the $YH_{1.7}+BP$ core is a better choice compared with other designs proposed in this paper as it provides a relatively high temperature margin.

KEYWORDS

heat pipe reactor, burnable poison, multiphysics analysis, hydrogen dissociation, monte-carlo method

1 Introduction

With the development of nuclear energy, micro reactors have received increasing interest among researchers in recent years. The main advantages of micro reactors are more flexibility in construction and deployment, better safety performance, and fewer operation requirements compared to large-scale nuclear power plants (Zohuri, 2020). Therefore, micro reactors have great application potential in the power supply of special scenarios, which is of great importance in developing revolutionary technology. Among the various micro reactor designs, Heat Pipe Reactors (HPRs) use heat pipe instead of the coolant circuit to export the heat out of the core (Yan et al., 2020). Compared with other reactor designs, HPRs have a simpler primary loop design with no flow system or flow auxiliary systems such as pumps and valves, which provide good mobility and plug-play availability. Moreover, HPRs possess inherent safety because of the passive heat conduction characteristics of the heat pipe (Mueller and Tsvetkov, 2021). Therefore, HPRs are considered to be an ideal choice for space power, deep-sea exploration, and power supply in remote regions (McClure et al., 2015; Maioli, 2019).

Under the non-proliferation requirement of civilian terrestrial nuclear reactor applications, the low-enrichment uranium fuel challenges the achievement of the criticality of HPRs. The introduction of moderators is considered to be an ideal choice, and metal hydrides are the most popular moderator materials for HPRs at present. In our previous work, based on the OpenMC model of one-sixth of the MegaPower core (Guo et al., 2021), a moderated megawatt-class HPR core design has been proposed to increase the power density and reduce fuel loading, core volume, and weight (Feng et al., 2022). Other research has also evaluated the effectiveness of various moderator materials such as matrix graphite, yttrium hydride, and uranium-zirconium hydride (Li et al., 2022; Li et al., 2023; Wu et al., 2023).

However, the moderated core usually exhibits larger burnup reactivity loss and higher excessive reactivity at the beginning of the lifetime, which poses challenges to core safety. Furthermore, although the hydrogen stability of the moderator rods under normal conditions has been verified in our previous work, the hydrogen dissociation risk of metal hydrides under accident conditions has not been effectively assessed.

This paper will focus on addressing the large burnup reactivity loss problem by the application of burnable poisons (BP) and assessing the hydrogen stability of metal hydride under accident conditions. Boron, gadolinium, and erbium are the most common burnable poison materials used in thermal spectrum reactors (Evans et al., 2022). As for fast reactors, the designs combining low-enriched boron-based burnable poison and moderators are also investigated (Guo et al., 2020). These burnable poison materials will be assessed in this paper. As for the hydrogen dissociation risk problem, the temperature field variation during the transient process needs to be obtained to assess the hydrogen stability under accident conditions. The transient analysis of HPRs under accident conditions requires consideration of multiple physical fields (Agung et al., 2013; Ma et al., 2021b). Researchers have also proposed several multi-physics coupling analysis methods based on different platforms, such as

RMC/ANSYS (Ma et al., 2021a; Ma et al., 2022), MOOSE (Matthews et al., 2021), and PRAGMA/OpenFOAM/ANLHTP (Im et al., 2023). In this work, a coupling method is developed based on OpenMC/ABAQUS with the point kinetic model to analyze the transient temperature response of the reactor under accident conditions, and the hydrogen stability of the moderator under accident conditions will be analyzed based on the temperature field and hydrogen dissociation criteria.

In this paper, Section 2 will describe the design of burnable poisons loaded in the moderated megawatt-class HPR core. Section 3 will discuss the safety characteristics of different designs during accident conditions, including reactivity insertion accidents, loss of power conversion unit (PCU) heat sink accidents, and heat pipe failure accidents. Finally, the conclusion and perspectives of this paper will be presented in Section 4.

2 Burnable poison design

2.1 BP design description

In our previous study, zirconium hydride was introduced as the moderator in the moderated core design (Mod. core) based on the reference MegaPower core (Ref. core). One-sixth of the Ref. core model consists of 204 potassium heat pipes and 352 fuel channels, containing 19.75 wt% enriched UO_2 fuel pellets (McClure et al., 2015). The Mod. core replaces all even rows of fuel rods, from inside to outside, with moderator rods, as shown in Figure 1. The $\text{ZrH}_{1.4}$ is chosen as the moderator in the Mod. core for analysis in this section. The open-source Monte Carlo neutron and photon transport simulation code OpenMC is chosen in this work to calculate the physical characteristics (Romano and Forget, 2013; Romano et al., 2015). The ENDF/B-VII.1 library is used as the cross-section library. The particles are set to 50,000. The batches are set to 500 with 50 inactive batches.

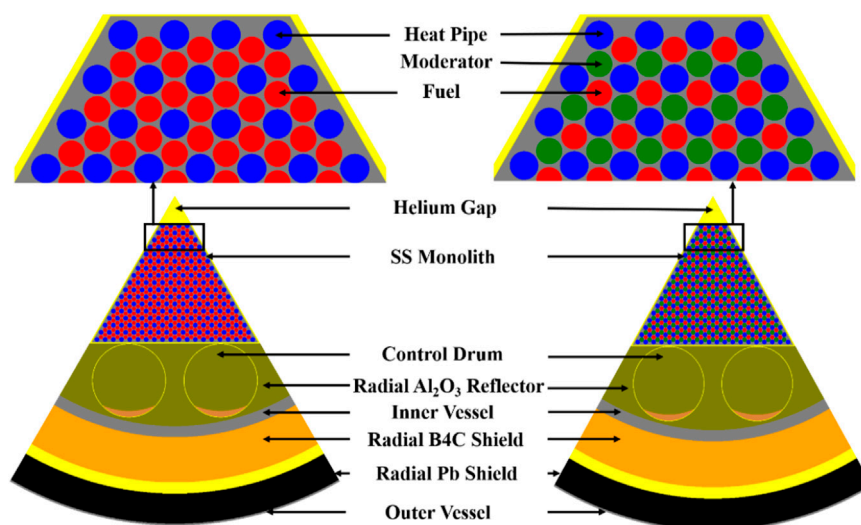
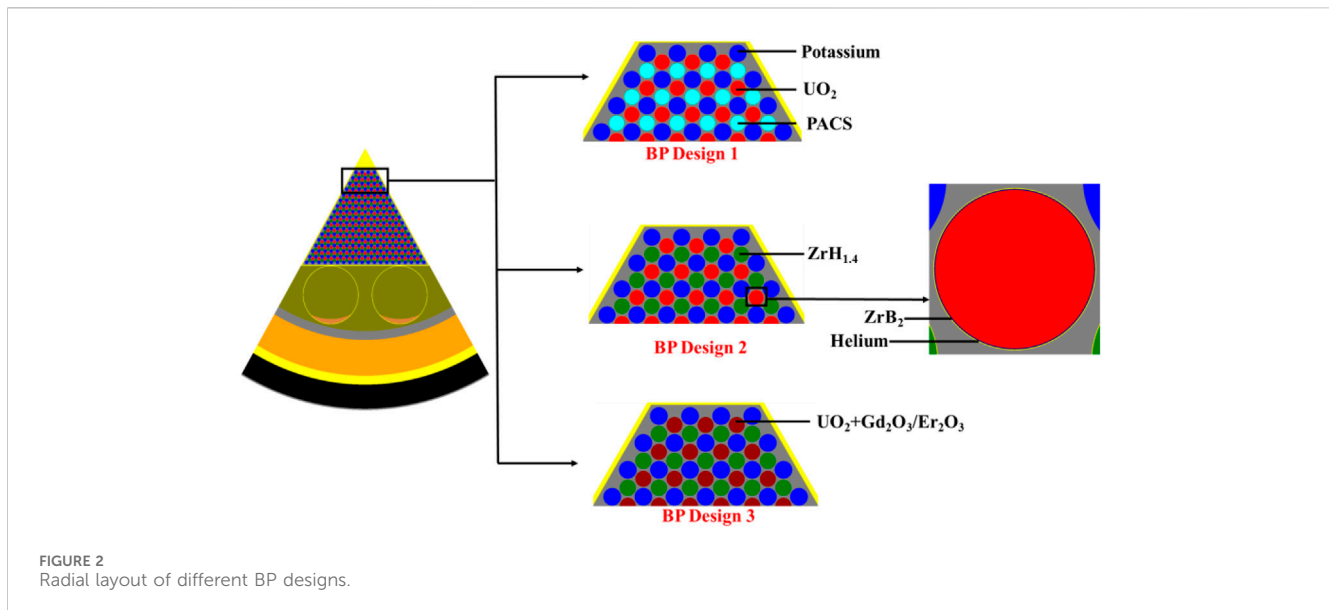


FIGURE 1
Radial layout of the Ref. core and the Mod. core (Feng et al., 2022).



As mentioned above, the introduction of metal hydrides can increase the power density and reduce the fuel loading as well as the core volume and weight. However, the burnup reactivity loss of the Ref. core and the Mod. core are separately -830 pcm and $-4,052$ pcm. A higher burnup reactivity loss and excessive reactivity at BOL pose significant safety challenges to the core. Therefore, the addition of BPs is a considerable option to compensate for the large burnup reactivity loss and excessive reactivity. In this section, 3 BP designs with different absorption materials are proposed. The core configuration of different designs are shown in Figure 2.

Based on the Mod. core, the BP design 1 replaces all $ZrH_{1.4}$ rods with polycarbaborane-siloxane-ethynyl (PACS) rods. PACS is a boron containing, high hydrogen polymer with strong thermal stability, being stable up to $1,000^{\circ}C$, and radiation resistance. The advantage of this design is that PACS rods can simultaneously serve as both moderator and BP, eliminating the need for additional design considerations. PACS-L is selected as the material of PACS rods, and the detailed composition of PACS-L can be seen from (Allen, 2003). A 0.1 mm ZrB_2 clad is coated on the surface of the fuel rods in the BP design 2 based on the Mod. core. Consequently, the radius of the fuel rods is reduced by 0.1 mm. As for the BP design 3, the discrete type BPs are used in the form of mixing with the UO_2 fuel. As the most common used discrete type BP materials, Gd_2O_3 and Er_2O_3 are selected and will be assessed in the following section.

2.2 BP performance assessment

Two parameters were adopted to assess the performance of different materials: burnup reactivity loss and k_{eff}^{EOL} , which is the core effective multiplication factor at end of life (EOL). The design objective is to minimize the burnup reactivity loss while ensuring k_{eff}^{EOL} is greater than 1. The calculations are conducted

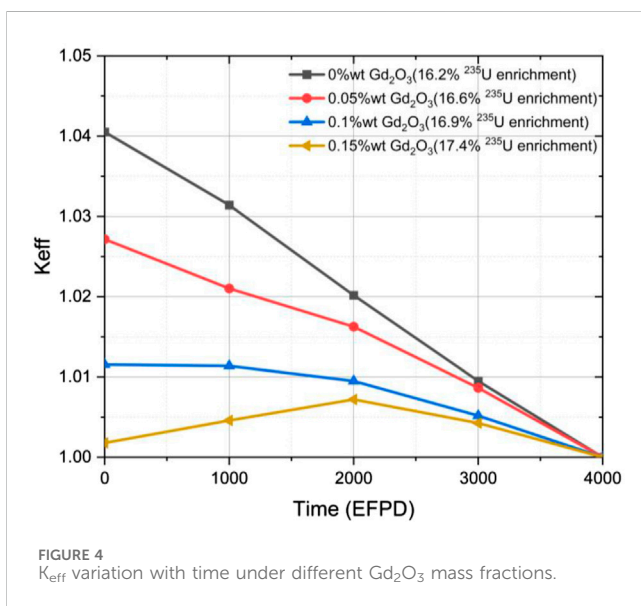
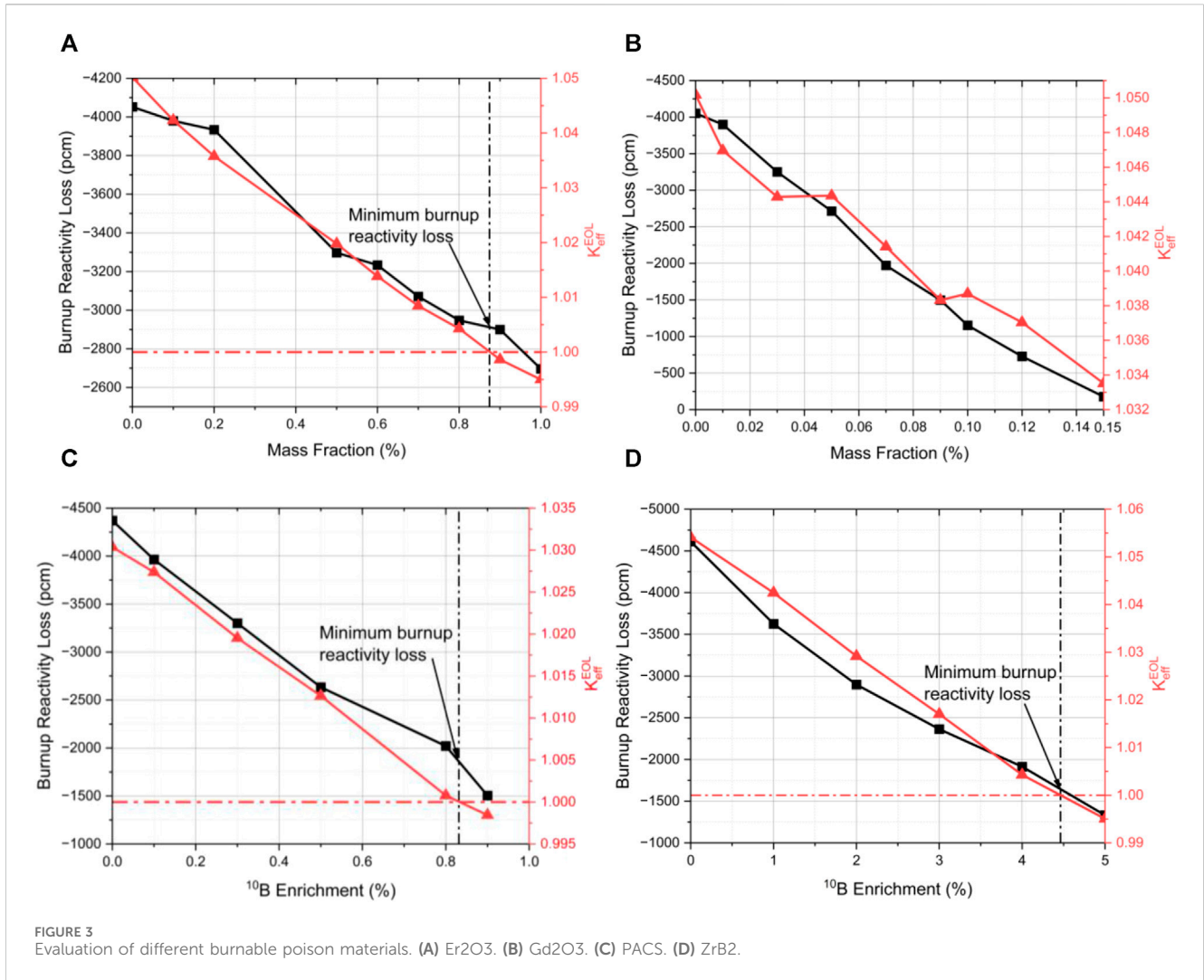
with 19.75 wt% enrichment of UO_2 . The results are shown in Figure 3.

It can be observed that the minimum burnup reactivity loss for Er_2O_3 , PACS, and ZrB_2 are separately $-2,900$ pcm, $-1,850$ pcm, and $-1,650$ pcm. While the three materials above can reduce the burnup reactivity loss, the effectiveness is limited. In contrast, Gd_2O_3 exhibits a better neutron absorption capacity, possessing lower burnup reactivity loss and higher k_{eff}^{EOL} . However, the excessive absorption capacity of Gd_2O_3 may lead to significant reactivity fluctuations or even increases during the lifetime. To determine a reasonable Gd_2O_3 mass fraction, the variation of K_{eff} with time under different mass fractions of Gd_2O_3 was calculated, and the results are shown in Figure 4. In Figure 4, the fuel enrichment under different Gd_2O_3 mass fractions is tuned to ensure the k_{eff}^{EOL} equals 1. The tuned fuel enrichment for 0%, 0.05%, 0.1%, and 0.15% mass fractions of Gd_2O_3 are separately 16.2%, 16.6%, 16.9%, and 17.4%.

It can be seen that the 0.15% mass fraction of Gd_2O_3 exhibits the minimum burnup reactivity loss, but the K_{eff} increases with time in the early stage of the lifetime, which makes reactivity control more complex. In fact, The K_{eff} will begin to increase with time as long as the Gd_2O_3 mass fraction is larger than 0.1% according to our calculation. As a result, the 0.1% mass fraction of Gd_2O_3 is selected as the burnable poison loaded in the core in this work, reducing the burnup reactivity loss from $-4,052$ pcm to $-1,154$ pcm. It should be noted that the addition of 0.1% mass fraction of Gd_2O_3 has little impact on the thermal properties of fuel (Iwasaki et al., 2009). Therefore, the influence of BPs on temperature field is assumed to be negligible.

3 Safety analysis

To assess the performance of different moderators, the transient response of $YH_{1.7}$, which possesses a similar hydrogen atom density as $ZrH_{1.4}$, moderated core with BP is also included in the analysis. The geometry of the $YH_{1.7}$ core with BP is the same as the $ZrH_{1.4}$ core with BP, except that all $ZrH_{1.4}$ rods have been replaced with



YH_{1.7} rods. Also, the BP loaded in the YH_{1.7} core is the 0.1% mass fraction of Gd₂O₃ mixed with fuel. The burnup reactivity loss of YH_{1.7} core with BP is -1,259 pcm. This section will analyze the hydrogen stability characteristics of the Ref. core, the ZrH_{1.4} moderated core without burnable poison (ZrH_{1.4} core), the ZrH_{1.4} moderated core with burnable poison (ZrH_{1.4}+BP core), and the YH_{1.7} moderated core with burnable poison (YH_{1.7}+BP core) under accident conditions.

Based on the Phenomena Identification and Ranking Table (PIRT) of the MegaPower reactor published by LANL (Sterbentz et al., 2017), several important issues related to the transient behavior are selected as the basic transient process analyzed in this section.

3.1 Methodology

3.1.1 Neutronics model

The OpenMC model and the depletion mesh layout are presented in Figure 5, where each fuel rod is divided into

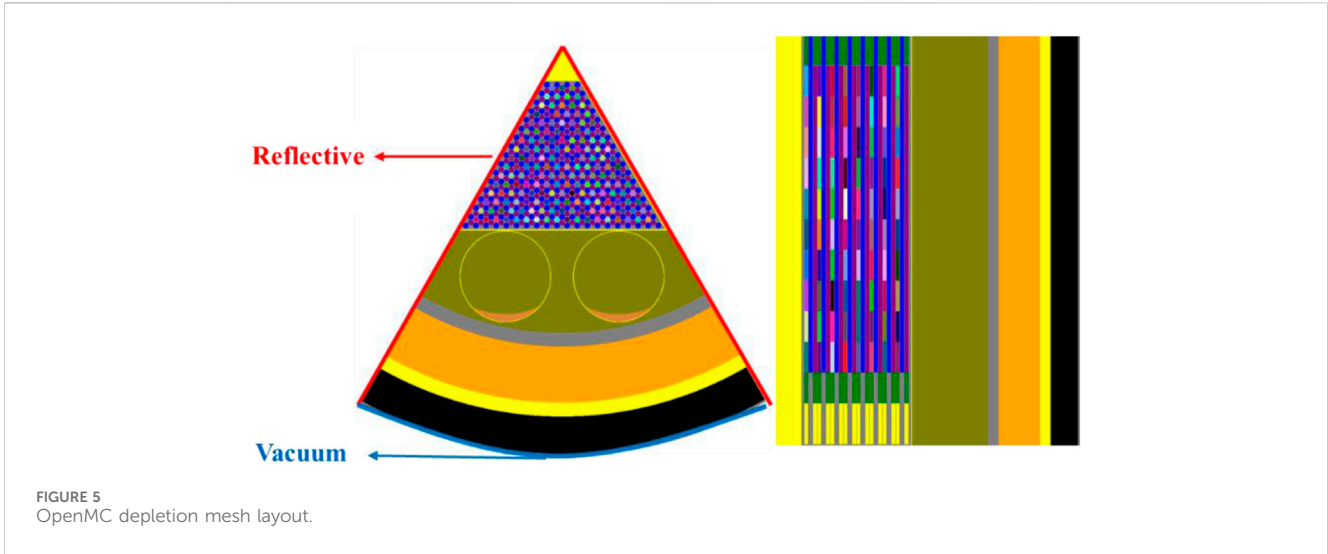
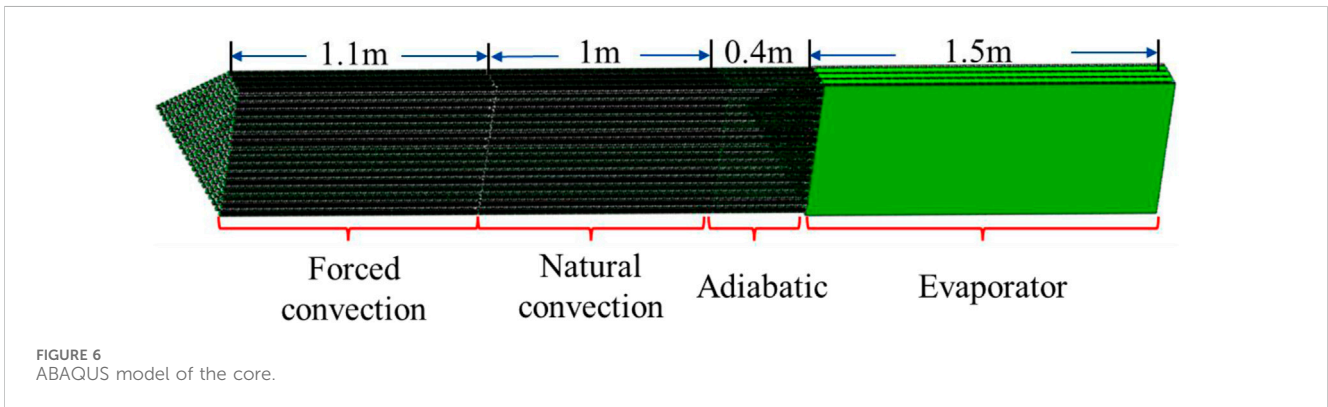


TABLE 1 The reactivity feedback coefficients of 4 cores.

Reactivity feedback coefficient (pcm·K ⁻¹)	Ref.	ZrH _{1.4}	ZrH _{1.4} +BP	YH _{1.7} +BP
Doppler effect	-0.64 ± 0.12	-1.72 ± 0.15	-1.58 ± 0.15	-1.51 ± 0.14
Thermal expansion of monolith	-1.97 ± 0.23	-0.53 ± 0.27	-0.74 ± 0.27	-0.74 ± 0.23
Thermal expansion of fuel	-0.68 ± 0.11	-0.27 ± 0.15	-0.31 ± 0.14	-0.31 ± 0.12
Thermal expansion of moderator	—	-0.73 ± 0.32	-0.57 ± 0.33	-0.82 ± 0.31



10 burnup zones in the axial direction. The reflective boundary condition is applied on the left and right surfaces of the model, while the vacuum boundary condition is applied on the surface of the outer stainless steel layer.

A point neutron kinetic model is used to calculate the power change of the core during the transient process. The reactor is considered as a lumped parameter system without changes in the flux spatial distribution during the transient, and the initial flux spatial distribution is given by OpenMC. The point neutron kinetic

equation with M groups delayed neutrons is described in Eq. (1) and Eq. (2):

$$\frac{dN(t)}{dt} = \frac{\rho(t) - \beta}{\Lambda} N(t) + \sum_{i=1}^M \lambda_i C_i(t) + Q, \quad (1)$$

$$\frac{dC_i(t)}{dt} = \frac{\beta_i}{\Lambda} N(t) - \lambda_i(t) \quad i = 1, 2, \dots, M, \quad (2)$$

where $N(t)$ is neutron flux, $C_i(t)$ is the concentration of the i th group delayed neutron precursors, β_i is the i th group delayed

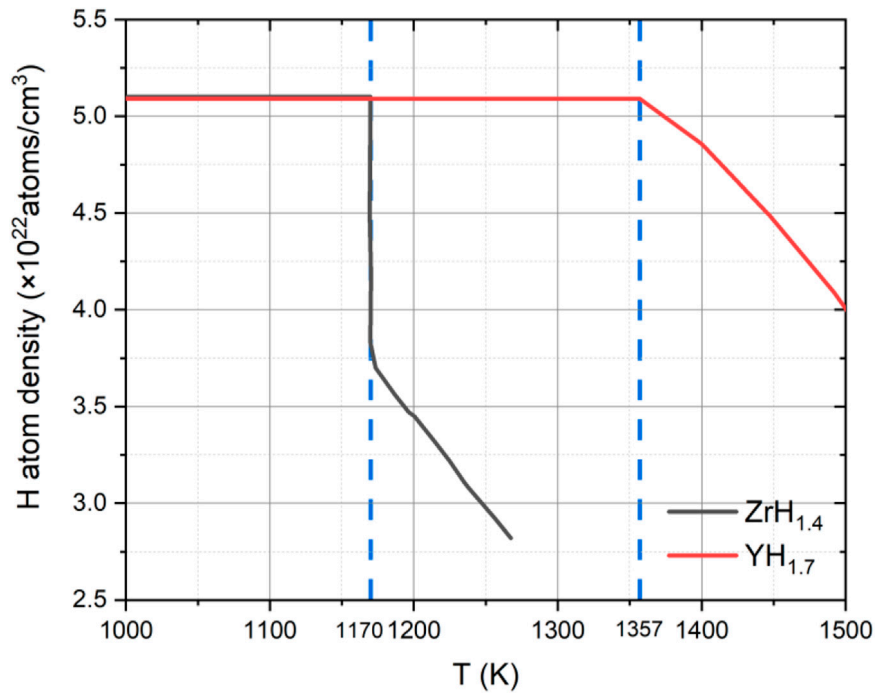


FIGURE 7 Hydrogen atom density variation of ZrH_{1.4} and YH_{1.7} with temperature.

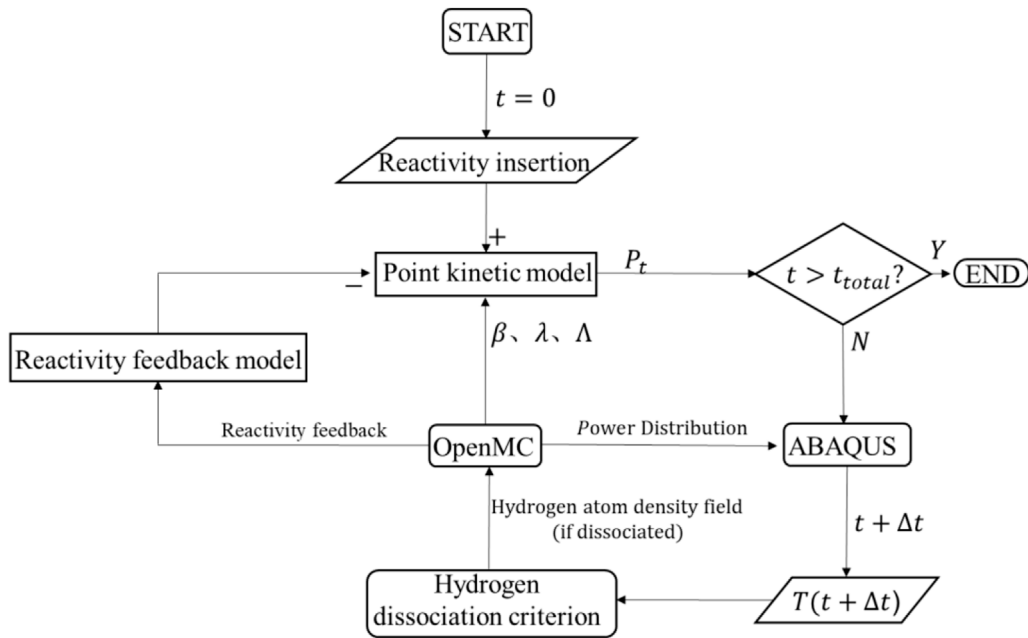


FIGURE 8 OpenMC/ABAQUS coupling scheme.

TABLE 2 Temperature limitation of fuel, moderator, and monolith.

Active core parts	Temperature limitation (K)
Fuel	2,800
Moderator	1,170 (for ZrH _{1.4})
	1,357 (for YH _{1.7})
Monolith	1,600

neutron fraction, λ_i is the decay constant of the i th group delayed neutron precursors, Λ is the generation time of prompt neutrons.

In this work, a six-group delayed neutron structure is used in the calculation. And the six-group delayed neutron kinetic parameters of 4 different designs used in this equation are calculated using OpenMC. Moreover, in the reactivity feedback model, the reactivity feedback coefficients of 4 different designs are also calculated using OpenMC, and will be used to calculate the negative reactivity feedback. The reactivity feedback coefficients of 4 different designs are shown in Table 1.

3.1.2 Thermal model

The temperature field of the core is analyzed using the finite element software ABAQUS. For this purpose, one-sixth of the reactor core sectors and the heat pipes are explicitly modeled in this work. The ABAQUS model of the core is illustrated in Figure 6.

As for the heat pipes, heat pipes are high thermal conductance devices which transfer heat by two-phase fluid circulation. The heat pipes transfer the heat from the Then the vapor flows to the condenser section, where it condenses and releases its latent heat. The liquid is drawn back to the evaporator section by capillary action, where it is re-vaporized to continue the cycle (Zohuri, 2016). In the thermal model, heat pipes are divided into 4 sections in the axial direction, which are the evaporator section (1.5 m), adiabatic section (0.4 m), natural convection condenser section (1 m), and forced convection condenser section (1.1 m). The convective boundary condition is applied on the outer surface of each heat pipe wall to represent the secondary loop heat exchanger. Under normal conditions, the forced convection condenser section of the heat pipe is used to export the heat out of the core, while the natural convection condenser section is not activated.

In this work, the effective thermal resistance network model with the solid assumption is applied in the heat transfer model of heat pipes. This effective model is commonly used and validated in many researches (Liu et al., 2020; Ma et al., 2020; Wang et al., 2020; Liu et al., 2022). According to (Zuo

and Faghri, 1998), the effective thermal conductivity coefficient of the wick region is written in Eq. (3):

$$k = \frac{k_l + k_s - (1 - \alpha)(k_l - k_s)}{k_l + k_s + (1 - \alpha)(k_l - k_s)} k_l, \tag{3}$$

where k_l is the thermal conductivity coefficient of the liquid working medium, k_s is the thermal conductivity coefficient of the solid material of the wick, α is porosity of the wick.

According to (Lienhard IV and J.H.), the effective thermal conductivity coefficient of the vapor region is written in Eq. (4):

$$\lambda(t) = \frac{\pi d_v^4 \rho^2 \gamma}{128 \mu T}, \tag{4}$$

where ρ is the density of the vapor working medium, γ is the latent heat of the liquid working medium, μ is the dynamic viscosity of the vapor working medium.

At normal conditions, the secondary loop is considered to extract the heat of the core. According to the thermal equilibrium calculation under normal conditions, the convective heat transfer coefficient of the forced convection condenser section is $446 \text{ W/m}^2 \cdot \text{K}$. The natural convection condenser section is considered to extract the core decay heat, which is 3% of the normal heat, so the convective heat transfer coefficient of the natural convection is $9 \text{ W/m}^2 \cdot \text{K}$ according to the thermal equilibrium calculation.

3.1.3 Hydrogen dissociation criteria

The introduction of metal hydride moderator rods brings the risk of significant hydrogen dissociation during accident conditions. When the hydrogen dissociation occurs in the majority of moderator rods within the reactor, a large amount of combustible hydrogen gas will be released into the reactor core, and, if not effectively addressed, the accumulation could lead to an explosion.

Therefore, in design criteria, it is required that the simultaneous significant hydrogen dissociation in the majority of moderator rods should not occur. In our previous research (Feng et al., 2022), the variation of hydrogen atom density of zirconium hydride and yttrium hydride with temperature has been obtained from (Vetrano, 1971; Zuzek et al., 1990), which will be used in this work as hydrogen dissociation criteria during accident conditions to determine whether the moderator rods dissociate.

The variation of the hydrogen atom density of ZrH_{1.4} and YH_{1.7} with temperature is shown in Figure 7. It can be seen that the ZrH_{1.4} rod begins to dissociate when the temperature reaches 1170 K. The YH_{1.7} rod has a larger temperature margin and does not dissociate until the temperature reaches 1357 K.

TABLE 3 Reactivity insertion values in different core designs.

	Ref.	ZrH _{1.4}	ZrH _{1.4} +BP	YH _{1.7} +BP
Excessive reactivity at BOL/pcm	830	4,052	1,154	1,259
Reactivity uncertainty/pcm	350	350	350	350
1 Drum reactivity at BOL/pcm	98	367	125	134

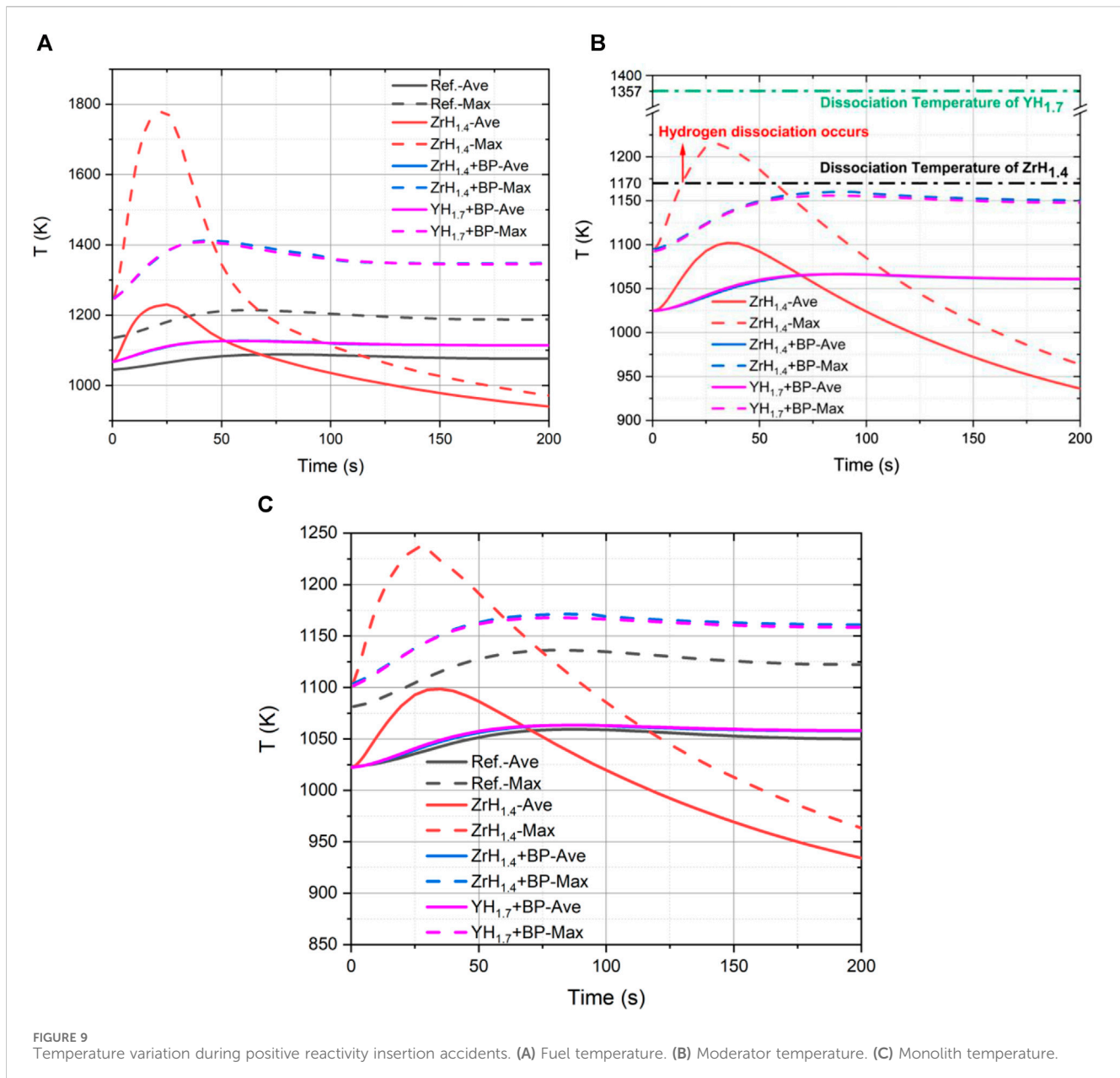


FIGURE 9 Temperature variation during positive reactivity insertion accidents. (A) Fuel temperature. (B) Moderator temperature. (C) Monolith temperature.

The variation of the hydrogen atom density with temperature shown in Figure 7 Serves two purposes:

- As the basis for determining whether hydrogen dissociation occurs. If the maximum temperature of moderator rods exceeds the limitation, the core is considered not satisfying the hydrogen dissociation criteria. This is also the core objective of safety analysis in this paper.
- Provides hydrogen density distribution for trend-based calculations of core changes after hydrogen dissociation. In the calculation after hydrogen dissociation occurs, it is assumed that the released hydrogen is removed from the core.

It should be noted that the released hydrogen distribution after dissociation in accident conditions is more complex than the simple hydrogen totally removed assumption. For example, the hydrogen diffusion, the hydrogen migration, and the permeation through the stainless steel of the monolith, etc., To obtain a more accurate depiction of core changes after hydrogen dissociation, a more refined model would be necessary.

After all, the primary focus of this paper remains on determining whether hydrogen dissociation occurs. As for the changes in the core after hydrogen dissociation, it merely provides a potential trend-based result based on the hydrogen totally removed assumption, as mentioned above.

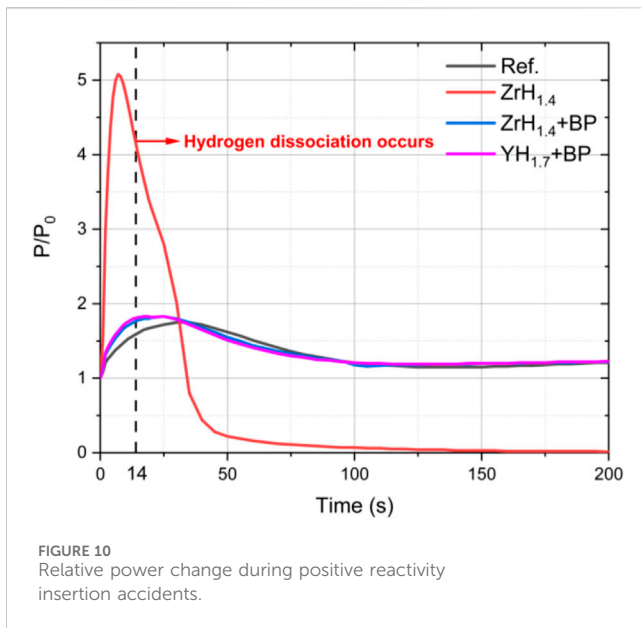


FIGURE 10
Relative power change during positive reactivity
insertion accidents.

3.1.4 OpenMC/ABAQUS coupling scheme

In this work, a coupling method is developed to integrate the OpenMC code and ABAQUS software with the point kinetic model, and reactivity feedback model to enable neutronic-thermal transient calculation. The schematic of the coupling method is shown in Figure 8.

The calculation begins from the steady-state result under normal conditions. The point kinetic model is used to obtain the power change at each time step, taking into account external reactivity insertion and reactivity feedback. The temperature field at every time step is calculated by ABAQUS, and then this data is transported to the hydrogen dissociation criterion to determine whether the moderator rods dissociate and calculate the hydrogen atom density distribution in dissociated moderator rods, which will be transported to the OpenMC model at the next time step. The whole calculation and data exchange process is controlled by a Python script.

3.1.5 Safety criteria

UO₂ is adopted as fuel in all the core designs, and the melting point of UO₂ is 3120 K. Considering that the burnup effect will decrease the melting point, the temperature limitation of fuel is set to 2800 K. As for the monolith material, the melting point of 316 stainless steel is around 1600 K, so the temperature limitation of monolith is set to 1500 K with a temperature margin of 100 K. The temperature limitation of moderator rods are defined by hydrogen dissociation criteria, which is 1170 K and 1357 K separately for ZrH_{1.4} and YH_{1.7}. The limitations are listed in Table 2.

3.2 Results and analysis

In this section, the transient response characteristics of the Ref. core, the ZrH_{1.4} core, the ZrH_{1.4}+BP core, and the YH_{1.7}+BP core

under accident conditions are calculated and analyzed. The focus of the analysis is the hydrogen stability of the moderator rods under accident conditions.

3.2.1 Positive reactivity insertion

Positive reactivity insertion due to accidental rotation of control drums is a basic accident of high importance in HPRs. In this work, the value of the reactivity insertion is considered to be the reactivity input caused by the accidental rotation of one single control drum at BOL. In this calculation, it is assumed that a single control drum rotates from the critical angle to the angle at which the absorber is completely away from the core.

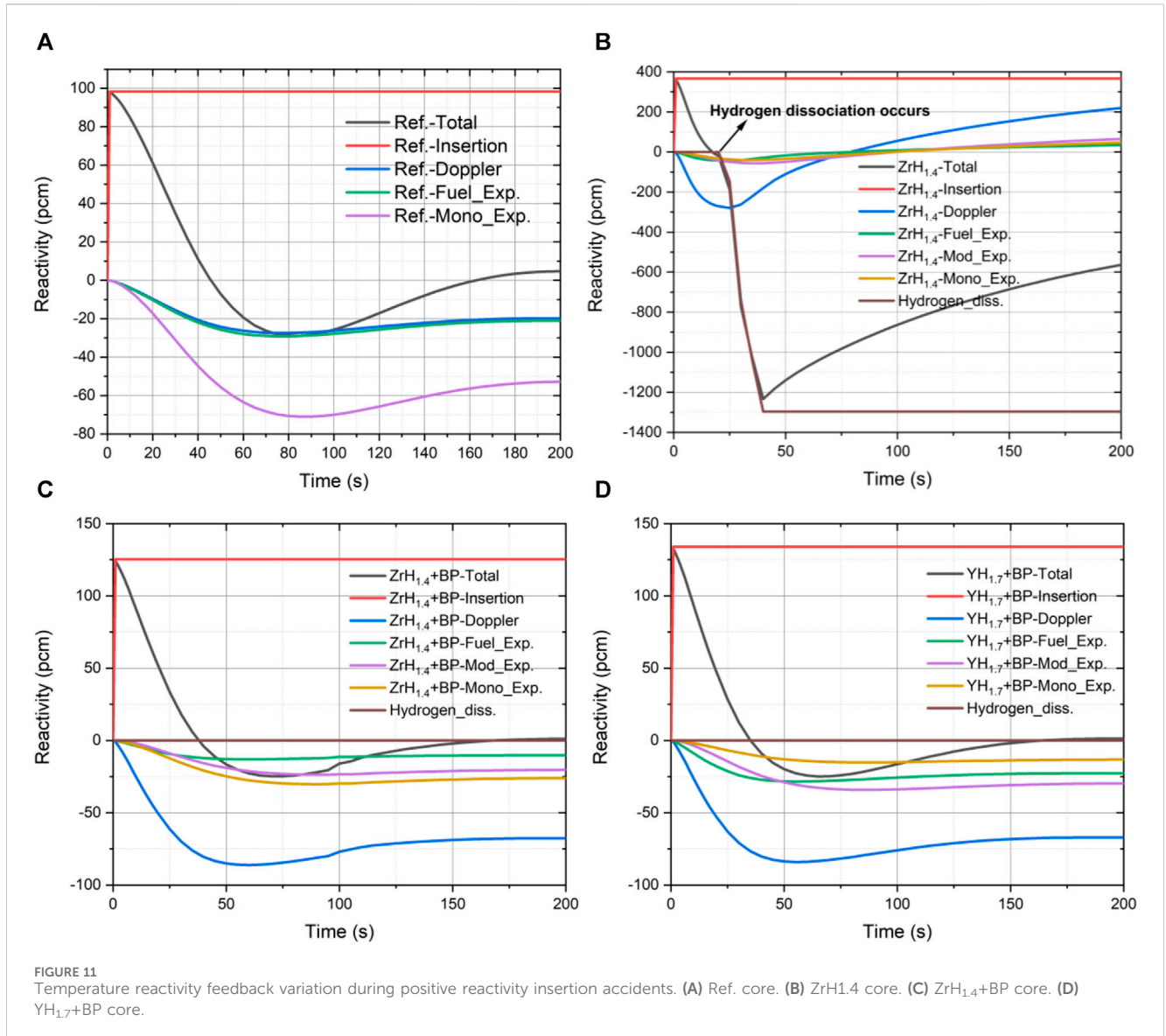
As a result, the values of reactivity insertion in different core designs are decided by the excessive reactivity of different designs at BOL, and are shown in Table 3. The values of excessive reactivity of Ref., ZrH_{1.4}, ZrH_{1.4}+BP, and YH_{1.7}+BP cores at BOL are separately 830 pcm, 4,052 pcm, 1,154 pcm, and 1,259 pcm. A reactivity uncertainty of 350 pcm is considered in this calculation. There are 12 control drums in each core design, so the reactivity values of single control drum accidental rotation are separately 98 pcm, 367 pcm, 125 pcm, and 134 pcm in the 4 core designs, which will be input to point kinetic model as external reactivity insertion in the subsequent calculation.

The variation of the average and maximum fuel, moderator, and monolith temperature of different cores during the transient is shown in Figure 9. Compared with designs loaded with burnable poisons, the ZrH_{1.4} core has a higher temperature peak during the accident. Moreover, the significant hydrogen occurs in the ZrH_{1.4} core at 14 s after the transient occurs, which not occur in the ZrH_{1.4}+BP core and YH_{1.7}+BP core. So it can be concluded that the ZrH_{1.4} core cannot satisfy the hydrogen dissociation criteria during the positive reactivity insertion accidents, while the introduction of burnable poisons can relieve this issue.

As for the other cores, the ZrH_{1.4}+BP core and YH_{1.7}+BP core exhibit similar trends in the average and maximum temperature during the accident, with the maximum temperature of 1410 K, 1160 K, and 1170 K separately for fuel, moderator, and monolith during the transient. Although the hydrogen dissociation does not occur in the ZrH_{1.4}+BP core, the safety margin for ZrH_{1.4} is exceptionally slim, being less than 10 K. In contrast, YH_{1.7} demonstrates a larger safety margin, making it a better choice.

Lastly, let's examine the variation of the core temperature of the ZrH_{1.4} core after hydrogen dissociation. Although these results are trend-based calculations under ideal conditions, the rapid decrease of core temperature also demonstrates the potential capability of rapid alleviation of accident consequences due to the negative reactivity feedback of hydrogen dissociation.

Figures 10, 11 display the relative power change and reactivity feedback of four different core designs during the positive reactivity insertion accident. As shown in Figure 10, the higher excessive reactivity in the ZrH_{1.4} core leads to a higher power peak, which causes a higher core temperature and hydrogen dissociation. However, after the introduction of



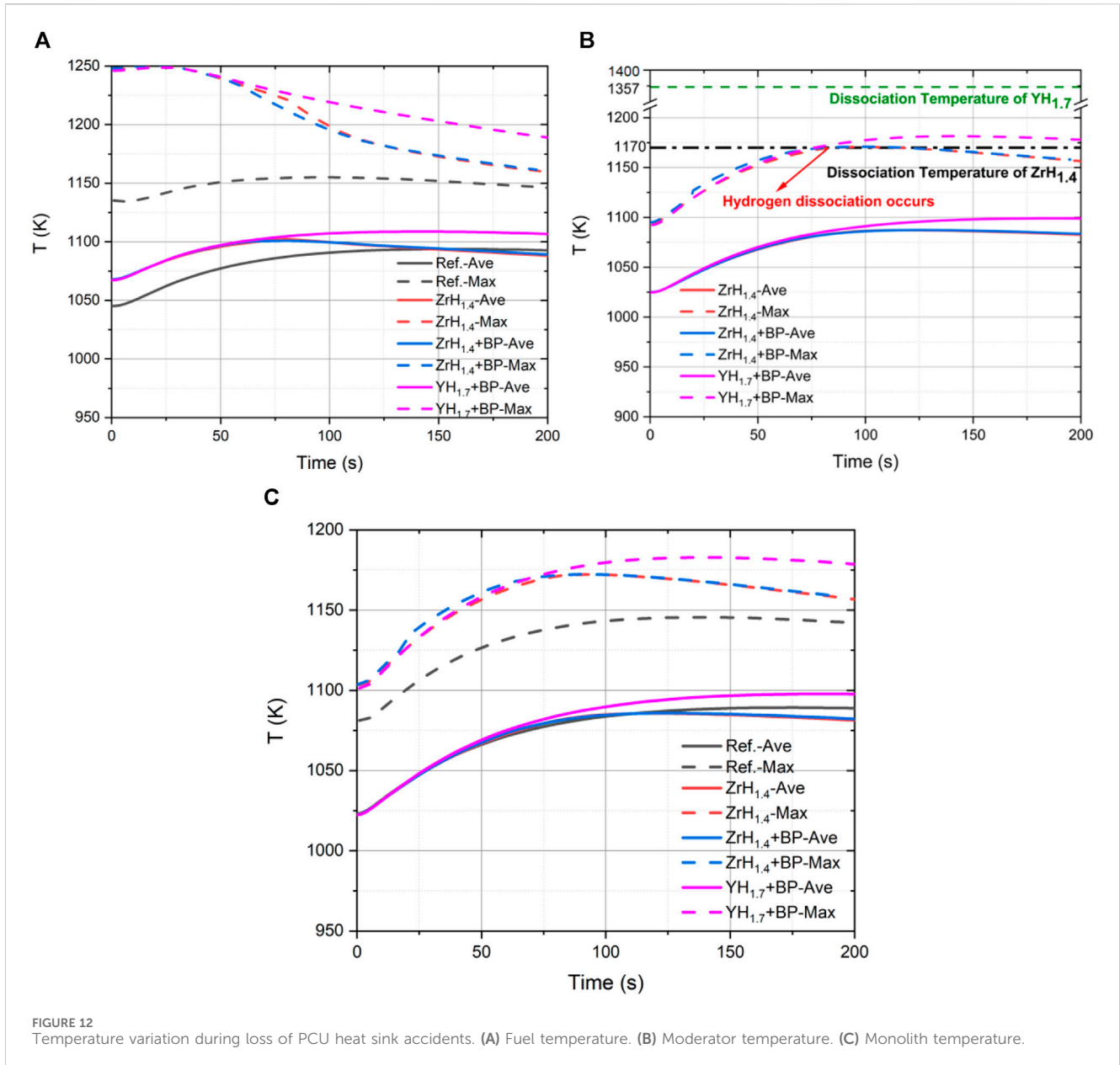
burnable poisons, the core exhibits power changes similar to those in the Ref. core, which shows better performance than the ZrH_{1.4} core. As for the reactivity feedback shown in Figure 11, it can be seen that the monolith expansion is the primary reactivity feedback mechanism in the Ref. core, while the major reactivity feedback mechanism of the ZrH_{1.4}+BP core and YH_{1.7}+BP core is the Doppler effect of fuel instead of the monolith expansion.

However, for the ZrH_{1.4} core, The occurrence of hydrogen dissociation renders it in violation of safety criteria. Similarly, the reactivity feedback after hydrogen dissociation depicted in Figure 11 is a trend with the assumptions. However it is intriguing to note the significant negative reactivity feedback introduced by hydrogen dissociation under these conditions.

3.2.2 Loss of PCU heat sink

In this section, the hydrogen stability of different core designs during the loss of the PCU heat sink without safety system conditions is calculated. In this accident, the HPs continue to remove heat from the core, but the natural air convection cools HPs instead of the forced air convection. To simulate this condition, the convective boundary condition at the forced convection condenser section is removed in the thermal model, and the convective boundary condition at the natural convection condenser section is activated.

The variation of the average and maximum fuel, moderator, and monolith temperature of the core during the loss of PCU heat sink accidents is shown in Figure 12. It can be seen that the ZrH_{1.4} will dissociate whether burnable poisons are introduced or not, while YH_{1.7} still exhibits a substantial temperature margin, approximately 170 K. As a result, the ZrH_{1.4} core and ZrH_{1.4}+BP core do not meet



the hydrogen stability criteria during the loss of PCU heat sink accidents.

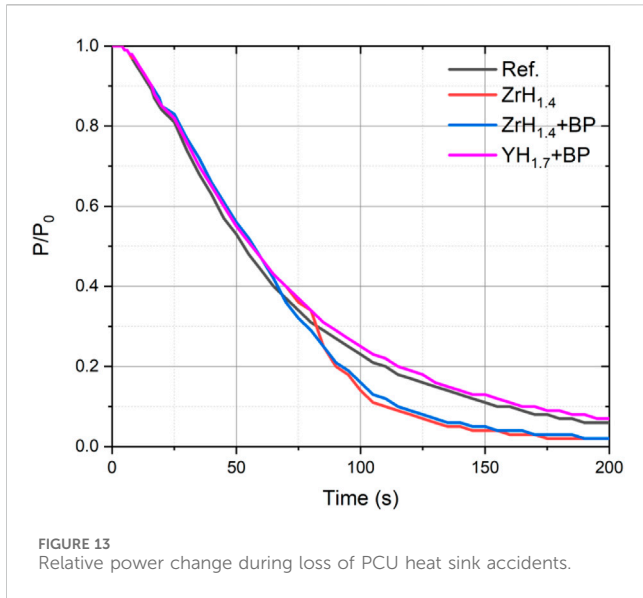
Meanwhile, it is noteworthy to examine the variations in fuel temperature. In contrast to the continuous increase in maximum fuel temperature observed in the Ref. core, the maximum fuel temperature in other cores decreases during the transient. The primary cause of this phenomenon is the enhancement of fuel Doppler effects due to the moderation of the neutron spectrum.

The relative power change and reactivity feedback of different core designs during the loss of PCU heat sink accidents is shown in Figures 13, 14.

It can be seen that the relative power of all the cores decreases with time and decays to about 0 due to the negative reactivity feedback of the core. The loss of PCU heat sink accidents will lead to a core shutdown in all core

designs. As for the reactivity feedback, the major reactivity feedback mechanism in the Ref. core is still the monolith expansion effect. For the $ZrH_{1.4}$ core and $ZrH_{1.4}+BP$ core, hydrogen dissociation occurs in both cores at approximately 75 s after the transient happens. For the $YH_{1.7}+BP$ core, it can be seen that although the $YH_{1.7}+BP$ core possesses a higher core temperature during the transient process, hydrogen dissociation does not occur in the moderator rods. The main negative reactivity feedback comes from the Doppler effect of fuel rods and the moderator expansion effect.

In summary, under the loss of PCU heat sink accident, the hydrogen dissociation occurs in both the $ZrH_{1.4}$ core and $ZrH_{1.4}+BP$ core, while the $YH_{1.7}+BP$ core will not experience hydrogen dissociation and exhibit a larger temperature margin.



3.2.3 Heat pipe failure

The heat pipe failure accident is also one of the essential basic accidents in HPRs (Ma et al., 2020). In this calculation, the disabled heat pipe adjacent to the hottest fuel rod is removed from the thermal model, and the adiabatic boundary condition is applied to the surface of the heat pipe hole.

A steady-state calculation is conducted, and the maximum temperature of fuel rods, monolith, and moderator rods under different conditions are summarized in Table 4 to evaluate the hydrogen stability. Results show that under 1 heat pipe failure accident, the ZrH_{1,4} core exhibits the highest temperature, and the hydrogen dissociation will not occur in moderator rods. However, under 2 heat pipes failure accident, the maximum temperature of ZrH_{1,4} rods exceeds the critical temperature of hydrogen dissociation, while YH_{1,7} rods will not dissociate. There are two cases in the event of 3 heat pipes failure accidents, namely the fuel-centered 3 heat pipes failure accident (case 1) and the moderator-centered 3 heat pipes failure accident (case 2). The results show that ZrH_{1,4} rods will dissociate in both cases, while

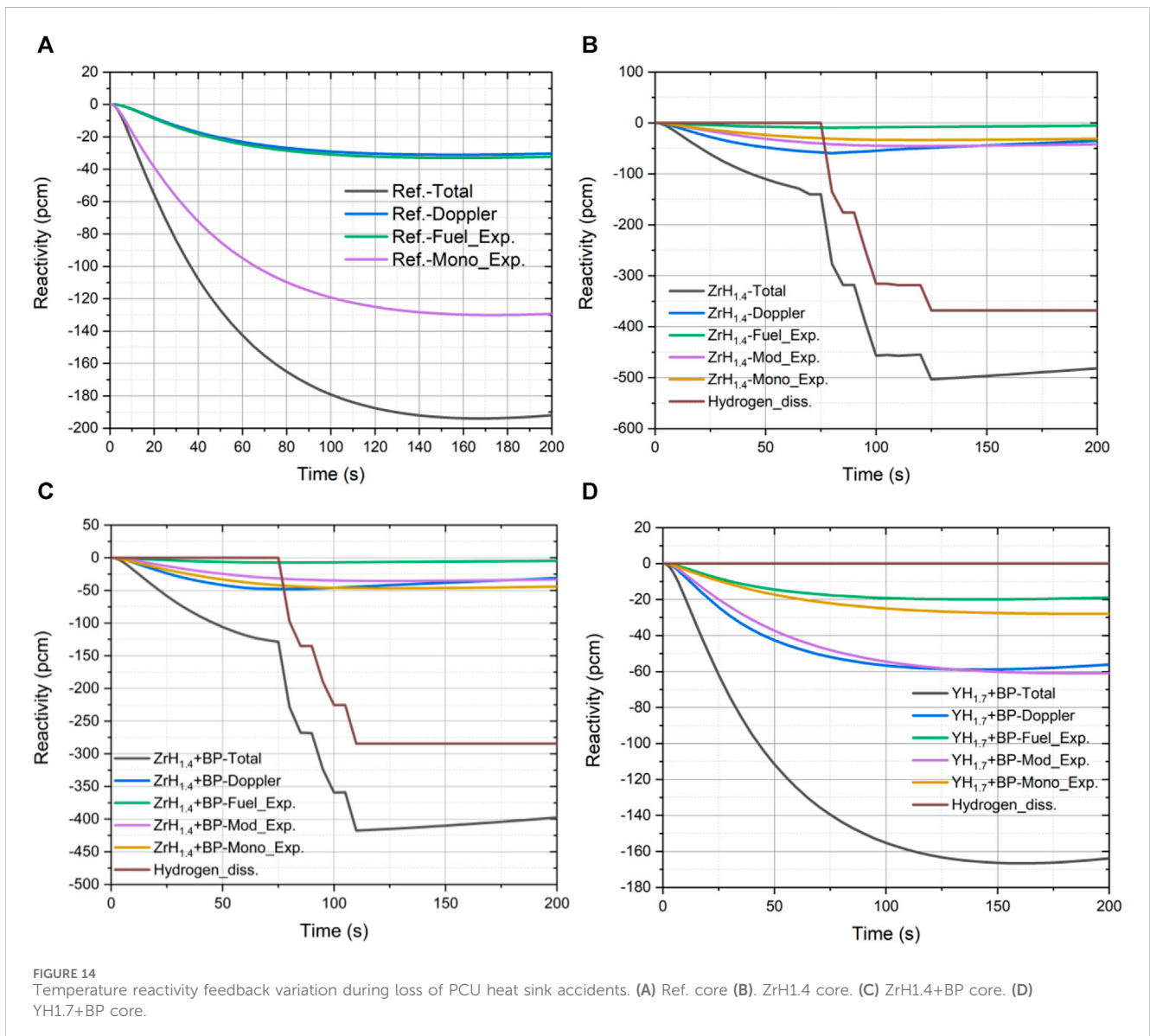
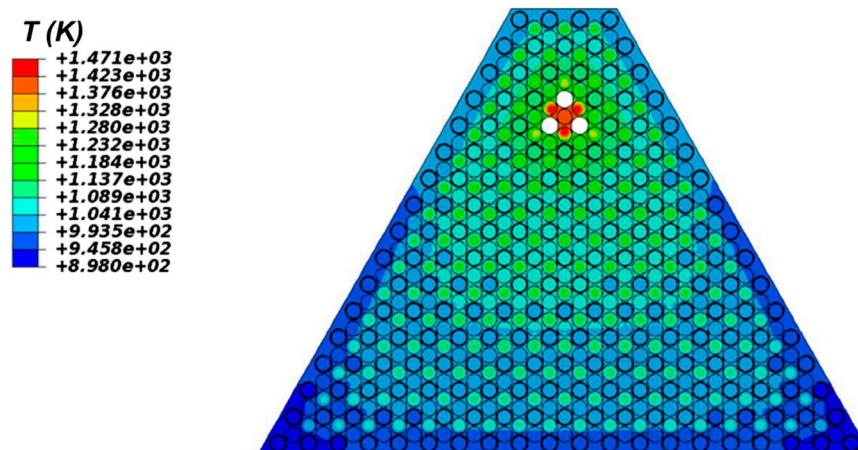


TABLE 4 The maximum core temperature under different conditions (unit: K).

		Ref.	ZrH _{1.4}	YH _{1.7}
Normal operating condition	Fuel	1,135	1,248	1,246
	Moderator	—	1,094	1,092
	Monolith	1,081	1,103	1,101
One heat pipe failure accident	Fuel	1,199	1,298	1,291
	Moderator	—	1,159	1,149
	Monolith	1,180	1,193	1,184
Two heat pipes failure accident	Fuel	1,386	1,375	1,360
	Moderator	—	1,250	1,233
	Monolith	1,292	1,261	1,245
Three heat pipes failure accident (case 1)	Fuel	1,488	1,500	1,471
	Moderator	—	1,299	1,273
	Monolith	1,412	1,333	1,307
Three heat pipes failure accident (case 2)	Fuel	1,488	1,470	1,455
	Moderator	—	1,401	1,386
	Monolith	1,412	1,407	1,393

FIGURE 15 Temperature field of YH_{1.7} core in three heat pipes failure accident (case 2).

YH_{1.7} rods will only dissociate in case 2. Figure 15 shows the temperature field of YH_{1.7} core in three heat pipes failure accident (case 2). It can be seen that only the YH_{1.7} rods in the center of three failed heat pipes exceeds the temperature limitation.

3.2.4 Summary

In summary, the introduction of burnable poisons can be beneficial during the positive reactivity insertion accident as it can reduce the excessive reactivity at BOL, thus reducing core temperature and preventing hydrogen dissociation in ZrH_{1.4} rods. However, during the loss of PCU heat sink accident, ZrH_{1.4} rods will dissociate regardless of the presence of burnable poisons,

whereas YH_{1.7} rods show better hydrogen stability. Moreover, in the event of the heat pipe failure accident, ZrH_{1.4} rods are more susceptible to dissociation than YH_{1.7} rods.

4 Conclusion

HPRs exhibit good mobility, plug-play availability, and inherent safety. Therefore, HPRs are considered to be an ideal choice for space power, deep-sea exploration, and power supply in remote regions. Metal hydride moderated HPRs are good solutions for critical problem under the non-proliferation requirement. However, the larger burnup

reactivity loss and hydrogen stability problems has not been effectively assessed. In this paper, a metal hydride moderated megawatt heat pipe reactor with burnable poisons is proposed, and the hydrogen stability is analyzed to assess the influence of moderator and burnable poisons. Gd_2O_3 is introduced as a burnable poison in the form of mixing with the UO_2 fuel. According to the results of the burnable poison design, the 0.1% mass fraction of Gd_2O_3 is selected as the burnable poison loaded in the core.

Safety analysis indicates that the introduction of burnable poisons can be beneficial during the positive reactivity insertion accident as it can reduce the excessive reactivity at BOL, thus reducing core temperature and preventing hydrogen dissociation in $ZrH_{1.4}$ rods. However, during the loss of PCU heat sink accident, $ZrH_{1.4}$ rods will dissociate regardless of the presence of burnable poisons, whereas $YH_{1.7}$ rods show better hydrogen stability. Moreover, in the event of the heat pipe failure accident, $ZrH_{1.4}$ rods are more susceptible to dissociation than $YH_{1.7}$ rods.

In conclusion, the introduction of burnable poisons is beneficial to reducing the core temperature and preventing moderator rods from hydrogen dissociation under the positive reactivity insertion accident. The $YH_{1.7}+BP$ core is a better choice overall as it provides a relatively high temperature margin.

However, the neutron-thermal-mechanics coupling analysis in the dynamic analysis is also needed for deeper analysis, which will be concluded in our future work. Moreover, the preliminary trend-based calculations of hydrogen dissociation show a intriguing negative hydrogen dissociation reactivity feedback, potentially helping to mitigate the consequences of severe accidents under ideal conditions, which can be further researched with more refined hydrogen models.

Data availability statement

The original contributions presented in the study are included in the article/Supplementary material, further inquiries can be directed to the corresponding author.

References

- Agung, A., Bánáti, J., Stálek, M., and Demazière, C. (2013). Validation of PARCS/RELAP5 coupled codes against a load rejection transient at the Ringhals-3 NPP. *Nucl. Eng. Des.* 257, 31–44. doi:10.1016/j.nucengdes.2012.12.023
- Allen, K. (2003). *An advanced burnable poison for pressurized water reactors*.
- Evans, J. A., DeHart, M. D., Weaver, K. D., and Keiser, D. D. (2022). Burnable absorbers in nuclear reactors – a review. *Nucl. Eng. Des.* 391, 111726. doi:10.1016/j.nucengdes.2022.111726
- Feng, K., Wu, Y., Hu, J., Jin, X., Gu, H., and Guo, H. (2022). Preliminary analysis of a zirconium hydride moderated megawatt heat pipe reactor. *Nucl. Eng. Des.* 388, 111622. doi:10.1016/j.nucengdes.2021.111622
- Guo, H., Buiron, L., Sciora, P., and Kooyman, T. (2020). Optimization of reactivity control in a small modular sodium-cooled fast reactor. *Nucl. Eng. Technol.* 52, 1367–1379. doi:10.1016/j.net.2019.12.015
- Guo, H., Feng, K. Y., Gu, H. Y., Yao, X., and Bo, L. (2021). Neutronic modeling of megawatt-class heat pipe reactors. *Ann. Nucl. Energy* 154, 108140. doi:10.1016/j.anucene.2021.108140
- Guo, H., Sciora, P., Kooyman, T., Buiron, L., and Rimpault, G. (2019). Application of boron carbide as burnable poison in sodium fast reactors. *Nucl. Technol.* 205, 1433–1446. doi:10.1080/00295450.2019.1620054
- Im, J., Jeong, M. J., Choi, N., Kim, K. M., Cho, H. K., and Joo, H. G. (2023). Multiphysics analysis system for heat pipe cooled micro reactors employing PRAGMA-

Author contributions

KF: Conceptualization, Investigation, Methodology, Software, Writing—original draft. JH: Data curation, Validation, Writing—review and editing. YW: Validation, Visualization, Writing—review and editing. TC: Supervision, Writing—review and editing. HG: Resources, Supervision, Writing—review and editing. HG: Conceptualization, Project administration, Supervision, Writing—review and editing.

Funding

The author(s) declare financial support was received for the research, authorship, and/or publication of this article. This study is sponsored by National Natural Science Foundation of China (Nos 12105170 and 12135008), Science and Technology on Reactor System Design Technology Laboratory, Shanghai Sailing Program (No. 20YF1420700), and the Future Foundation of the Energy Science. The computations in this paper were run on the π 2.0 cluster supported by the Center for High-Performance Computing at Shanghai Jiao Tong University.

Conflict of interest

The authors declare that the research was conducted in the absence of any commercial or financial relationships that could be construed as a potential conflict of interest.

Publisher's note

All claims expressed in this article are solely those of the authors and do not necessarily represent those of their affiliated organizations, or those of the publisher, the editors and the reviewers. Any product that may be evaluated in this article, or claim that may be made by its manufacturer, is not guaranteed or endorsed by the publisher.

OpenFOAM-ANLHTP. *Nucl. Sci. Eng.* 197, 1743–1757. doi:10.1080/00295639.2022.2143209

Iwasaki, K., Matsui, T., Yanai, K., Yuda, R., Arita, Y., Nagasaki, T., et al. (2009). Effect of Gd_2O_3 dispersion on the thermal conductivity of UO_2 . *J. Nucl. Sci. Technol.* 46, 673–676. doi:10.1080/18811248.2007.9711574

Li, J., Cai, J., and Li, X. (2023). Conceptual design and feasibility analysis of a megawatt level low enriched uranium heat pipe cooled reactor core. *Ann. Nucl. Energy* 181, 109576. doi:10.1016/j.anucene.2022.109576

Li, S., Yan, B., Tang, G., Peng, D., and Lu, H. (2022). "Preliminary design and neutronics analysis for a medium temperature heat pipe cooled reactor," in Student Paper Competition. Presented at the 2022 29th International Conference on Nuclear Engineering (American Society of Mechanical Engineers). Virtual, Online 015T16A017. doi:10.1115/ICONE29-89659

Liu, L., Liu, B., Xiao, Y., Gu, H., and Guo, H. (2022). Preliminary thermal and mechanical analysis on the reactor core of a new heat pipe cooled reactor applied in the underwater environment. *Prog. Nucl. Energy* 150, 104306. doi:10.1016/j.pnucene.2022.104306

Liu, X., Zhang, R., Liang, Y., Tang, S., Wang, C., Tian, W., et al. (2020). Core thermal-hydraulic evaluation of a heat pipe cooled nuclear reactor. *Ann. Nucl. Energy* 142, 107412. doi:10.1016/j.anucene.2020.107412

Ma, Y., Chen, E., Yu, H., Zhong, R., Deng, J., Chai, X., et al. (2020). Heat pipe failure accident analysis in megawatt heat pipe cooled reactor. *Ann. Nucl. Energy* 149, 107755. doi:10.1016/j.anucene.2020.107755

- Ma, Y., Liu, J., Yu, H., Tian, C., Huang, S., Deng, J., et al. (2022). Coupled irradiation-thermal-mechanical analysis of the solid-state core in a heat pipe cooled reactor. *Nucl. Eng. Technol.* S173857332200002X. 54, 2094–2106. doi:10.1016/j.net.2022.01.002
- Ma, Y., Liu, M., Xie, B., Han, W., Yu, H., Huang, S., et al. (2021a). Neutronic and thermal-mechanical coupling analyses in a solid-state reactor using Monte Carlo and finite element methods. *Ann. Nucl. Energy* 151, 107923. doi:10.1016/j.anucene.2020.107923
- Ma, Y., Tian, C., Yu, H., Zhong, R., Zhang, Z., Huang, S., et al. (2021b). Transient heat pipe failure accident analysis of a megawatt heat pipe cooled reactor. *Prog. Nucl. Energy* 140, 103904. doi:10.1016/j.pnucene.2021.103904
- Maoioli, A. (2019). *Westinghouse eVinci micro-reactor licensing modernization Project demonstration*. Southern Company. SC-29980-202.
- Matthews, C., Laboure, V., DeHart, M., Hansel, J., Andrs, D., Wang, Y., et al. (2021). Coupled Multiphysics simulations of heat pipe microreactors using DireWolf. *Nucl. Technol.* 207, 1142–1162. doi:10.1080/00295450.2021.1906474
- McClure, P. R., Poston, D. I., Dasari, V. R., and Reid, R. S. (2015). *Design of megawatt power level heat pipe reactors (No. LA-UR-15-28840)*. Los Alamos, NM (United States): Los Alamos National Lab. LANL. doi:10.2172/1226133
- Mueller, C., and Tsvetkov, P. (2021). A review of heat-pipe modeling and simulation approaches in nuclear systems design and analysis. *Ann. Nucl. Energy* 160, 108393. doi:10.1016/j.anucene.2021.108393
- Romano, P. K., and Forget, B. (2013). The OpenMC Monte Carlo particle transport code. *Ann. Nucl. Energy* 51, 274–281. doi:10.1016/j.anucene.2012.06.040
- Romano, P. K., Horelik, N. E., Herman, B. R., Nelson, A. G., Forget, B., and Smith, K. (2015). OpenMC: a state-of-the-art Monte Carlo code for research and development. *Ann. Nucl. Energy* 82, 90–97. doi:10.1016/j.anucene.2014.07.048
- Sterbentz, J. W., Werner, J. E., McKellar, M. G., Hummel, A. J., Kennedy, J. C., Wright, R. N., et al. (2017). *Special purpose nuclear reactor (5 MW) for reliable power at remote sites assessment report (No. INL/EXT-16-40741)*. Idaho Falls, ID (United States): Idaho National Lab. doi:10.2172/1410224
- Une, K. (1986). Thermal expansion of UO_2 - Gd_2O_3 fuel pellets. *J. Nucl. Sci. Technol.* 23, 1020–1022. doi:10.1080/18811248.1986.9735090
- Vetrano, J. B. (1971). Hydrides as neutron moderator and reflector materials. *Nucl. Eng. Des.* 14, 390–412. doi:10.1016/0029-5493(70)90159-7
- Wang, C., Sun, H., Tang, S., Tian, W., Qiu, S., and Su, G. (2020). Thermal-hydraulic analysis of a new conceptual heat pipe cooled small nuclear reactor system. *Nucl. Eng. Technol.* 52, 19–26. doi:10.1016/j.net.2019.06.021
- Wu, Y., Zheng, Y., Tao, Y., Liu, X., Du, X., and Wang, Y. (2023). The low-enriched uranium core design of a MW heat pipe cooled reactor. *Nucl. Eng. Des.* 404, 112195. doi:10.1016/j.nucengdes.2023.112195
- Yan, B. H., Wang, C., and Li, L. G. (2020). The technology of micro heat pipe cooled reactor: a review. *Ann. Nucl. Energy* 135, 106948. doi:10.1016/j.anucene.2019.106948
- Zohuri, B. (2016). *Heat pipe design and Technology: modern applications for practical thermal management*. Cham: Springer International Publishing. doi:10.1007/978-3-319-29841-2
- Zohuri, B. (2020). Nuclear micro reactors: the next wave of innovation. *Nucl. Micro React.*, 1–39. doi:10.1007/978-3-030-47225-2_1
- Zuo, Z. J., and Faghri, A. (1998). A network thermodynamic analysis of the heat pipe. *Int. J. Heat. Mass Transf.* 41, 1473–1484. doi:10.1016/S0017-9310(97)00220-2
- Zuzek, E., Abriata, J. P., San-Martin, A., and Manchester, F. D. (1990). The H-Zr (hydrogen-zirconium) system. *Bull. Alloy Phase Diagr.* 11, 385–395. doi:10.1007/BF02843318